DOI: 10.1002/adma.201606091

Article type: Communication

Author Manuscript

Monolithic Flexible Supercapacitors Integrated into Single Sheets of Paper and Membrane via Vapor Printing

*Andong Liu, Peter Kovacik, Nolan Peard, Wenda Tian, Hilal Goktas, Jonathan Lau, Bruce Dunn and Karen K. Gleason**

A. Liu, Dr. P. Kovacik, W. Tian, Dr. H. Goktas, Prof. K. K. Gleason

Department of Chemical Engineering

Massachusetts Institute of Technology

77 Massachusetts Avenue, Cambridge, MA 02139, USA

Email: kkg@mit.edu

N. Peard

Department of Mathematics

Massachusetts Institute of Technology

77 Massachusetts Avenue, Cambridge, MA 02139, USA

J. Lau, Prof. B. Dunn

Department of Materials Science and Engineering

University of California, Los Angeles

Los Angeles, CA 90095, USA

This is the author manuscript accepted for publication and has undergone full peer review but has not been through the copyediting, typesetting, pagination and proofreading process, which may lead to differences between this version and the Version of Record. Please cite this article as doi: 10.1002/adma.201606091.

This article is protected by copyright. All rights reserved.

Keywords: chemical vapor deposition, supercapacitors, printed electronics, conducting polymers, electrode-electrolyte interfaces

A novel approach to fabricate supercapacitors (SCs) via vapor printing, specifically oxidative chemical vapor deposition (oCVD), is demonstrated. Compared to stacking multiple layers into a SC, our method enables the monolithic integration of all components into a single-sheet substrate, minimizing the inactive materials and eliminating the possibility of multilayer delamination. Electrodes comprised of pseudo-capacitive material, poly(3,4-ethylenedioxythiophene) (PEDOT), are deposited into both sides of a sheet of flexible porous substrate. The film deposition and patterning are achieved in a single step. The oCVD PEDOT penetrates partially into the porous substrate from both surfaces while leaving the interior of the substrate serving as separator. Near the surface, the PEDOT coating conforms to the substrate's structure without blocking the pores, resembling the substrate's intrinsic morphology with high surface area. The porously structured PEDOT coating, paired with in situ ion gel electrolyte synthesis, gives enhanced electrode-electrolyte interfaces. The monolithic device demonstrates high volumetric capacitance (11.3 F cm^{-3}), energy density (2.98 mWh cm^{-3}) and power density (0.42 Wh cm^{-3}). These outstanding performance metrics are attributed to the large loading of active materials, minimization of inactive materials, and good electrode-electrolyte interfaces. SC arrays can be printed on a single substrate without the use of wire interconnects.

Author Manuscript

This article is protected by copyright. All rights reserved.

Flexible lightweight and wearable energy storage is critically important for the development of next-generation electronics.[1–3] Next generation energy storage is specifically desired to achieve the efficient combination of energy-harvesting devices, such as photovoltaics and piezoelectrics, with functional end-user interfaces, such as responsive sensors and circuits.[4–7] Supercapacitors (SCs) are a class of energy storage devices, prized for their high power densities. Flexible solid-state SCs are particularly promising for achieving compact, lightweight, and reliable energy storage.[5] Despite the enormous advancements in nanostructured electrode materials and functional electrolytes, until now, flexible SC devices still face challenges arising from the limitations of architectural design.[8] Current architectures rely predominantly on the layered "sandwich-like" structure, in which different components (e.g. cathode, separator, anode, and optional current collectors) are fabricated separately and then assembled by stacking. This stacking approach can compromise quality of the interfaces between the components and negatively affect the mechanical integrity of the SC.[9] The use of multiple, discrete substrates also adds unnecessary volume and weight to the device, decreasing its volumetric as well as gravimetric capacity. Furthermore, when multiple stacking-based SCs are combined into an array for specific voltage and capacitance rating, wire interconnects are often used, reducing the mechanical integrity even further. Advanced writing/printing-based fabrication techniques such as photolithography, laser writing, and inkjet printing have been applied, which diversified the SC cell designs and improved device integration.[8,10–13] Nevertheless, microfabrication processes face a challenge of low-cost and high-throughput scalability. Moreover, most of these works employed an "in-plane" configuration, which utilizes only one side of the substrate. Opportunities to take advantages of both sides of a substrate using writing/printing-based

Author Manuscript

This article is protected by copyright. All rights reserved.

techniques, boosting the volumetric energy and power densities with respect to the volume of entire device, have not been fully exploited.

We present a novel solid-state design in which all the components of a sandwich-like SC are monolithically integrated into a single substrate, eliminating the possibility of multilayer delamination. The integrated architecture relies on polymeric electrodes deposited into both sides of a single sheet of flexible porous substrate. The electrodes penetrate partially, but not fully, into the flexible substrate. Thus, the interior of the substrate can function as a separator and a solid-state electrolyte reservoir. Both electrodes comprise of pseudo-capacitive conducting polymer grown by oxidative chemical vapor deposition (oCVD).[14] Combining the oCVD with a stencil mask enables the vapor printing of electrode arrays, in which the film deposition and patterning occur in a single step. SCs in various circuit configurations can be easily vapor-printed on a single substrate by manipulating a shadow mask pattern. This work can open up opportunities to integrate vapor-printed energy storage device with vapor-printed photovoltaics fabricated by the same techniques on the same substrate,[15] leading to a flexible monolithic tandem system.

With the vapor-phase deposition process for the electrodes, we can control the conformality of the coating coverage and therefore the degree to which the coating penetrates into porous substrates.[16] The partially conformal coverage achieved using our approach,[17] as schematically shown in Figure S1b, is desirable for constructing SC devices. The conformal nature of the coating allows the utilization of the large surface area of porous substrate and contributes to the large

Author Manuscript

This article is protected by copyright. All rights reserved.

loading of active materials. Meanwhile, the finite vapor penetration depth into the porous substrate ensures separation of the electrodes deposited from the opposite sides of a substrate, thus prevents electrical shorting. To our best knowledge, the combination of these previously mutually exclusive characteristics has not yet been demonstrated. For comparison, commonly used solution-based coatings of paper and textile substrates suffer from poor control of the coating depth caused by wetting effects.[13] Further, we demonstrated that a secondary porous structure can be formed by fine-tuning the oCVD condition. To make the most of the hierarchically porous electrode, we utilized in situ ion gel synthesis method to incorporate solid-state electrolyte, enabling the formation of excellent electrode-electrolyte interfaces. We show that the monolithic device fabricated has outstanding energy and power densities, resulting from the large loading of active materials, the minimization of inactive materials and the exceptional interfaces.

The materials, fabrication procedure and intermediate/final configurations of our vapor-printed solid-state SC device are schematically depicted in **Figure 1**a. To demonstrate the versatility of our approach, two flexible and porous substrates were used and compared – general purpose cellulose filter paper (FP) and porous nylon membrane (NM). The FP was selected to demonstrate the compatibility of vapor printing with common and inexpensive substrates; the NM was selected due to its high porosity, large specific surface area, uniform morphology and robustness, together allowing fabrication of devices with state-of-the-art performance. The fabrication procedure consisted of three main steps i-iii: i. Gold current collectors (c.a. 100 nm) were sputtered onto both sides of the porous substrate to enhance electron transport to/from the pseudo-capacitive electrodes. The substrate was initially pre-treated by silanization with (3-

Author Manuscript

This article is protected by copyright. All rights reserved.

mercaptopropyl)trimethoxysilane in order to promote its adhesion to gold. The intermediate configuration of the SC after this step is shown in Figure 1a (i); ii. Electrodes of poly(3,4-ethylenedioxythiophene) (PEDOT), a known pseudo-capacitive material,[18–22] were deposited onto the current collectors via oCVD followed by methanol rinsing to eliminate excessive oxidant. During the oCVD process, the polymerized thin films were formed via simultaneous exposure to vapor-phase monomer (EDOT) and oxidant ($FeCl_3$) at low substrate temperatures (~ 50 °C) and moderate vacuum (for more details, see SI and Ref. [14]). The configuration after treatment step ii is shown in Figure 1a (ii); iii. Homogeneous mixture of ionic liquid [EMIM][BF_4], monomer N, N-dimethylacrylamide (DMAA), crosslinker ethylene glycol dimethacrylate (EGDMA), and thermal initiator 1.0 wt% of 4,4'-azobis(4-cyanovaleric acid) (ABCVA) ([EMIM][BF_4]/DMAA/EGDMA = 150/50/1, v/v/v) was drop-cast on the electrode (see SI for more details). The mixture of precursors spontaneously wetted through the electrodes and substrate. Ion gel electrolyte was then in situ synthesized inside the PEDOT electrodes and substrate via thermally initiated polymerization of the vinyl monomers at 90 °C. Figure 1a (iii) shows the final device configuration.

The surface morphology of the substrates was examined after each treatment step. Figure 1b (i-iii) shows the surfaces of the FP and Figure 1c (i-iii) the surfaces of the NM after the fabrication step i-iii. Both substrates before electrode printing (Figure 1b (i) and 1c (i)) feature porous surfaces with large surface area suitable for high energy and high power SC performances. The surface of the FP (Figure 1b (i)) is composed of coarse cellulose fibers (~20 µm diameter). In contrast, the NM (Figure 1c (i)) displays exceptionally fine and uniform porous structure (~5 µm features). Accordingly, the BET surface area of the bare NM (3.22 $m^2 g^{-1}$) is substantially higher than that of the bare FP (1.28 $m^2 g^{-1}$).

Author Manuscript

This article is protected by copyright. All rights reserved.

This fine and uniform structure of larger surface area underpins the superior device performance, which will be shown in the latter sections.

The morphological changes of the surfaces after PEDOT electrode printing are shown in Figure 1b (ii) and Figure 1c (ii). Specifically, in Figure 1b (ii), the smaller pores and fibers of the FP are less prominent after PEDOT deposition. This indicates the presence of the PEDOT coating, which is thick enough to fill the smaller pores. To compare, in Figure 1c (ii), the PEDOT coating appears more uniform, due to the underlying uniform porous structure of the NM substrate on which the PEDOT was coated. For both substrates, the PEDOT deposited via oCVD evenly coats the substrate surface and conforms to the outer texture of substrate.[17] The conformal nature of the PEDOT coating allows the large loading of active materials into some depth of the substrates' 3D network; at the same time, it ensures that the pores are not fully blocked off by the PEDOT layer. These open pores allow the penetration of gel electrolyte precursors in step iii, and the formation of good interface between electrode and gel electrolyte. A major challenge associated with the direct integration of electrodes into the opposite sides of a thin porous substrate is the potentiality of an electrical short across the substrate. Therefore, control of the degree of coating conformality is key to the successful integration of electrodes in our SC device fabrication. To illustrate the importance of conformality control, three representative scenarios of conformality are schematically illustrated in Figure S1. In the case of full conformality, PEDOT coating thickness would be uniform across the thickness of porous substrate (Figure S1a); In the case of non-conformal coverage, coatings would form two slab layers on top of either side of substrate (Figure S1c). Coating with full conformality gives large surface area, but connects the two electrodes and results in an electrical short. On the other hand,

Author Manuscript

This article is protected by copyright. All rights reserved.

non-conformality ensures the segregation of electrodes, but minimizes the surface area of coating, which would jeopardize the high power character of the SC device. Therefore, for our purpose to monolithically integrate two electrodes into opposite sides of a substrate, the partially conformal coverage (Figure S1b), an intermediate situation, would be most beneficial, allowing the utilization of porous structure for high surface area coating and high materials loading, but simultaneously ensuring effective electrode segregation. Facile conformality control is a key advantage of polymer CVD techniques over other deposition techniques.[16,17] Adjustment of oCVD parameters allows formation of coatings with partial conformality and ensures that the degree of coating penetration is limited to less than half the thickness of the substrates. This is done by maintaining the partial pressure of vapor-delivered oxidant sufficiently close to its saturation pressure. Since oCVD is a dry process, there are no wettability effects that could cause the undesirable penetration of the reactants throughout the thickness of the porous substrate. In comparison, solution-based coating process often has less control of coating conformality, allowing the free penetration of active materials through wetting. Techniques, such as pre-treatment of the substrates with hydrophobic coating, need to be employed to suppress the uncontrolled wetting.[13] The penetration of the oCVD PEDOT into a FP and NM can be directly observed from the cross-sectional energy dispersive X-ray spectroscopy (EDS) mapping of the sulfur present only in PEDOT (**Figure 2**b and 2d respectively). The clean cross-sections with minimal distortion, as shown in Figure 2a and 2c were prepared by embedding the sample in ice and freeze-fracturing the entire slab (Cryo-Snap).[23] It is confirmed that the PEDOT coating is restricted approximately in the top 30 µm depth of either side for the FP-based device, and 10 µm depth for the NM-based device, leaving gaps of 110 and 60 µm, respectively, in

Author Manuscript

This article is protected by copyright. All rights reserved.

between. The electrochemical performance of the fabricated device shown in the latter section of this article further confirms the effective segregation of the electrodes.

The microstructure of PEDOT electrodes can be optimized by fine-tuning the oCVD deposition conditions. A high oxidant-to-monomer ratio was set in order to generate a secondary porous structure. Despite the coating appearing smooth in Figure 1b (ii) and 1c (ii) at low magnification, the high-resolution SEM image of oCVD PEDOT, shown in Figure 2e, indicates the formation of a secondary porous structure inside the PEDOT coating. Consistent with the morphology, the BET surface area of the NM with oCVD PEDOT (~ 9.49 $m^2 g^{-1}$) increased significantly from that of the bare NM substrate (~ 3.22 $m^2 g^{-1}$), confirming the formation of the secondary structure with larger surface area. Hypothetically, the unreacted oxidant presented inside the structure functioned as a porogen. The excessive oxidant residues were dissolved and rinsed out by methanol, leaving the secondary pores behind. The secondary pores provided for expanded pathways for the infusion of the electrolyte into the electrodes and therefore larger electrode-electrolyte interfacial areas.

The method to incorporate the SC electrolyte was tailored to take the full advantage of the hierarchically porous electrode. It has been reported previously that extended solid electrode-electrolyte interface can be formed by soaking porous electrode with inviscid monomer-electrolyte mixture and subsequently initiating in situ polymer electrolyte gelation.[24] Here, we took a similar approach, and carefully selected the precursors of the gel: ionic liquid [EMIM][BF_4], monomer DMAA, crosslinker EGDMA, and thermal initiator ABCVA. [EMIM][BF_4] was chosen because of its

Author Manuscript

This article is protected by copyright. All rights reserved.

ability to dope/de-dope PEDOT and its wide electrochemical window.[19] DMAA is a highly polar monomer, promising to form gel with [EMIM][BF_4], with the trace crosslinker EGDMA to enhance the system's robustness. ABCVA is a low temperature initiator showing good miscibility with other precursors. It would allow a homogenous initiation at non-destructively thermal condition. The precursor mixture formed was substantially less viscid than pure [EMIM][BF_4]. It readily infiltrated the hierarchically porous PEDOT electrodes and the substrate when drop-cast. Upon thermal initiation, the solid-state gel electrolyte coating was in situ synthesized uniformly across the electrodes and substrate. The FTIR spectrum of a separately prepared freestanding gel pellet (Figure S2) presents characteristic bands of both pDMAA and [EMIM] [BF_4],[25,26] confirming the composition of the ion gel (see SI for detailed band assignments). The transparent presentation of the ion gel (Figure S2 inset) illustrates the gel's homogeneity and the absence of micro-phase separation. The SEM image of PEDOT surface after ion gel incorporation is shown in Figure 2f. Compared to the as-deposited PEDOT in Figure 2e, the solid-state electrolyte infiltrated the secondary pores of the PEDOT (but not the primary pores of the substrates), and partially smoothened the electrode surface. The X-ray photoelectron spectroscopy (XPS) results (Figure S3) show that the electrode after ion gel incorporation presents substantially reduced sulfur peak (~164 eV) belonged to PEDOT, indicating an even electrolyte coating on the surface of the PEDOT

The electrochemical performance of the vapor-printed SCs was assessed with cyclic voltammetry (CV), galvanostatic (GV) cycling, and electrochemical impedance spectroscopy (EIS) analyses. The results are normalized to the total volume of the entire monolithically integrated device, which is arguably the more realistic measure of the device performance.[5] **Figure 3**a and 3b show the CV

Author Manuscript

This article is protected by copyright. All rights reserved.

curves for the FP- and NM-based SCs at scan rates ranging from 25 to 200 mV s^{-1} within a potential range from 0 to 1.4 V versus the open circuit voltage. The CV curves of FP and NM-based SCs are nearly symmetric rectangular, except for some rounding at higher scan rates. The GV curves of the SCs over the voltage window of 0 to 1.4 V are presented in Figure 3c and Figure 3d. Both devices exhibited typical triangle-shape profiles and small IR drops (0.07 - 0.27 V for the FP-based device and 0.02 - 0.1 V for the NM-based device, see Figure S5 for enlarged view of IR drops) with cycling current densities from 0.16 to 0.64 A cm^{-3}.

Electrochemical impedance spectra (EIS) obtained for both devices using a 10 mV applied AC voltage from 50 kHz to 10 mHz are fitted to the equivalent circuit in Figure 3e inset. They are shown to be in good agreement with the fitting (Figure 3e). The low frequency tails imply the capacitive behaviors and confirm the absence of short. From the circuit fitting, the equivalent series resistances (ESRs) of the FP- and NM-based SCs are calculated to be 8.4 and 1.3 Ω, respectively. The charge transfer resistances from impedance fitting are calculated to be 0.59 and 0.38 Ω in the FP- and NM-based SCs, respectively, demonstrating the high quality of interfaces created through oCVD and the in situ gel electrolyte synthesis.

Comparing these results for the two SCs, it is notable that the NM-based device demonstrates less rounding of the CV curves, smaller IR drops, lower ESR, and lower charge transfer resistance. The better performance is solely due to the difference in morphology of the substrate materials. The NM has a finer and more uniform structure (~ 5 μm diameter features), and greater surface area (3.22

Author Manuscript

This article is protected by copyright. All rights reserved.

$m^2 g^{-1}$) than the FP (~ 20 µm diameter fibers, 1.28 $m^2 g^{-1}$), resulting in an increased PEDOT loading and improved ion-transport kinetics in the final device. These findings underscore the impact of substrate morphology on SC device performance, despite the same electrode and electrolyte materials.

Specific capacitances based on the volume of the entire integrated devices (thickness of 170 µm and 80 µm for the FP-based and the NM-based devices, respectively) were calculated from the GV curves and are compared with state-of-the-art performances for solid-state flexible SCs in Figure 3f.[27–30] The FP-based SC reaches specific capacitance of 3.92 F cm^{-3} at the current density of 0.16 A cm^{-3}, which is comparable to the previous reports; the NM-based SC is superior, reaching 11.3 F cm^{-3} at the current density of 0.16 A cm^{-3}, and demonstrating some of the highest reported volumetric capacitances. When the current density was increased from 0.16 to 0.64 A cm^{-3}, ~ 90% of the capacitance was retained for both SCs. The good rate capability can be attributed to the excellent electrode-electrolyte interface. In addition, the specific gravimetric capacitance based on mass of PEDOT materials was calculated to range from 70 to 75 F g^{-1} (Figure S6), which is consistent with the intrinsic values reported in literature.[21] The energy and power densities of the FP- and NM-based SCs are presented in the Ragone plot (**Figure 4**a). Our vapor-printed SCs, maintaining the high power characteristic of SCs, achieves a volumetric energy density of ~2.98 mWh cm^{-3}, which is comparable to the recently reported values for supercapacitors and the thin-film batteries (0.3-10 mWh cm^{-3}).[29–31]

Author Manuscript

This article is protected by copyright. All rights reserved.

The FP-based SC demonstrates reasonably good capacity retention of 83% after 8,000 cycles using GV over 0 to 1.2 V (Figure 4b). The capacitance lost was recovered by adding two external carbon paper current collectors. This finding suggests that the loss originates from the degradation of the gold current collectors, rather than the PEDOT. This finding is consistent with the previous reports that imidazolium-based ionic liquids can slowly corrode gold.[32,33] Subsequent works to enhance capacitance retention will be focused on seeking more compatible electrolyte and/or improving the retention of current collector. The performance of the vapor-printed SC was not significantly affected by the mechanical bending to a certain angle (Figure 4c). Also shown in the same figure, after being flexed 1,000 times, the device exhibits only ~7% capacitance loss. The mechanical flexibility of our SC can be attributed to the integration of the PEDOT and gel electrolyte into the intrinsically flexible substrate. Our monolithic scheme eliminates the possibility of layer delamination. To compare, the multilayers of a stacked sandwich-type SC would incur relative displacement during the consecutive bending cycles, which may cause the delamination of the device.[9]

The excellent performances of the vapor-printed supercapacitors can be attributed to the advantages of our novel SC configuration. First, large amount of active materials is effectively incorporated into the 3D structure of the porous substrate, owing to the partially conformal nature of the coatings synthesized via oCVD. In comparison, with the previous works on printed SC, the penetration of "ink" into the 3D structure of substrate needed to be intentionally hindered. [8,13] As a result, the loading of active materials onto the substrate was limited and the fabrication of devices failed to utilize the intrinsic morphology of the substrate. Meanwhile, the partial conformality,

Author Manuscript

This article is protected by copyright. All rights reserved.

rather than full conformality, ensures the effective separation of electrodes on both sides, and thus allows the utilization of both sides of the substrate for electrode printing. The use of the inactive substrate in this configuration, compared to that in the in-plane configuration, is reduced. Lastly, the hierarchically porous electrode structure generated via oCVD, paired with in situ ion gel electrolyte synthesis, generates excellent electrode-electrolyte interfaces and ensures fast ion-transport kinetics.

Depending on the specific application, multiple SCs need to be connected in series and/or parallel, similarly as batteries are, to form a power source supplying desired voltage and current. One of the most appealing features of vapor-printed integrated SCs is the versatility to vary the device layout by simple manipulation of mask pattern, which eliminates the use of wire interconnects. The vapor-printed SCs can be connected in complex series or/and parallel configurations without sacrificing the integrity of the combined device. As illustrated in Figure 4d, by varying the mask patterns for both sides, series (2S), parallel (2P) and series/parallel (2S2P) connections can be fabricated, to achieve specific voltage and discharging time for the printed device (Figure 4e). Last but not least, a large scale vapor-printed SC (12×12 cm^2) was fabricated and is shown in Figure 4f, thanks to the recent demonstration of the scalability of oCVD.[34]

To conclude, we developed a novel monolithically integrated SC design enabled by oCVD. Pseudo-capacitive PEDOT is synthesized into both sides of single sheets of porous substrate, with the inner part of the substrate functioning as separator. While the oCVD PEDOT gives a conformal coverage

Author Manuscript

This article is protected by copyright. All rights reserved.

allowing for utilization of large surface area of the porous substrate and large loading of active materials, its finite vapor penetration depth ensures separation of the electrodes and thus prevents shorting. We demonstrated the applicability of our method on filter paper, representing the inexpensive substrates, and porous nylon membrane, representing performance optimized morphology. We used in situ ion gel synthesis method for the solid-state electrolyte incorporation. We show that the monolithic device has excellent specific volumetric capacitance, power density, and energy density, due to the large loading of active materials, minimization of inactive materials, and good electrode-electrolyte interface formed. SCs in various circuit configurations can be easily printed on a single substrate. This work provides opportunities to print both energy storage device and photovoltaics via the same vapor-based techniques on a single substrate, towards the monolithic integration of energy supply for a self-powered system.

Supporting Information

Supporting Information is available from the Wiley Online Library or from the author.

Acknowledgements

The authors acknowledge financial support from the Office of Naval Research under Contract N00014-13-1-0466. Hongmou Zhang from Department of Urban Studies and Planning at MIT is acknowledged for help with the visuals. We also thank Jonathan Shu from the Cornell Center for Materials Research (CCMR) for asssitance with XPS measurements. This work made use of the CCMR Research Shared Facilities which are supported through the NSF MRSEC program (DMR-1120296).

Author Manuscript

This article is protected by copyright. All rights reserved.

Received: ((will be filled in by the editorial staff))
Revised: ((will be filled in by the editorial staff))
Published online: ((will be filled in by the editorial staff))

Author Manuscript

[1] Y. Gogotsi, *Nature* **2014**, *509*, 568.

[2] D. Yu, K. Goh, H. Wang, L. Wei, W. Jiang, Q. Zhang, L. Dai, Y. Chen, *Nat. Nanotechnol.* **2014**, *9*, 555.

[3] Y. Shao, M. F. El-Kady, L. J. Wang, Q. Zhang, Y. Li, H. Wang, M. F. Mousavi, R. B. Kaner, *Chem. Soc. Rev.* **2015**, *44*, 3639.

[4] S. Pan, J. Ren, X. Fang, H. Peng, *Adv. Energy Mater.* **2016**, *6*, DOI 10.1002/aenm.201501867.

[5] X. Lu, M. Yu, G. Wang, Y. Tong, Y. Li, *Energy Environ. Sci.* **2014**, *7*, 2160.

[6] L. Dong, C. Xu, Y. Li, Z. H. Huang, F. Kang, Q. H. Yang, *J. Mater. Chem. A* **2016**, *4*, 4659.

[7] Y.-Z. Zhang, Y. Wang, T. Cheng, W.-Y. Lai, H. Pang, W. Huang, *Chem. Soc. Rev.* **2015**, *44*, 5181.

[8] K.-H. Choi, J. Yoo, C. K. Lee, S.-Y. Lee, *Energy Environ. Sci.* **2016**, 2812.

[9] K. Wang, X. Zhang, C. Li, X. Sun, Q. Meng, Y. Ma, Z. Wei, *Adv. Mater.* **2015**, *27*, 7451.

[10] Z. Niu, L. Zhang, L. Liu, B. Zhu, H. Dong, X. Chen, *Adv. Mater.* **2013**, *25*, 4035.

[11] M. F. El-Kady, R. B. Kaner, *Nat. Commun.* **2013**, *4*, 1475.

[12] Y. Xu, M. G. Schwab, A. J. Strudwick, I. Hennig, X. Feng, Z. Wu, K. Müllen, *Adv. Energy Mater.*

This article is protected by copyright. All rights reserved.

2013, *3*, 1035.

[13] L. Hu, H. Wu, Y. Cui, *Appl. Phys. Lett.* **2010**, *96*, 2008.

[14] S. G. Im, K. K. Gleason, *Macromolecules* **2007**, *40*, 6552.

[15] M. C. Barr, J. A. Rowehl, R. R. Lunt, J. Xu, A. Wang, C. M. Boyce, S. G. Im, V. Bulovic, K. K. Gleason, *Adv. Mater.* **2011**, *23*, 3500.

[16] S. H. Baxamusa, K. K. Gleason, *Chem. Vap. Depos.* **2008**, *14*, 313.

[17] A. M. Coclite, R. M. Howden, D. C. Borrelli, C. D. Petruczok, R. Yang, J. L. Yagüe, A. Ugur, N. Chen, S. Lee, W. J. Jo, A. Liu, X. Wang, K. K. Gleason, *Adv. Mater.* **2013**, *25*, 5392.

[18] J. M. D'Arcy, M. F. El-Kady, P. P. Khine, L. Zhang, S. H. Lee, N. R. Davis, D. S. Liu, M. T. Yeung, S. Y. Kim, C. L. Turner, A. T. Lech, P. T. Hammond, R. B. Kaner, *ACS Nano* **2014**, *8*, 1500.

[19] M. Ghaffari, S. Kosolwattana, Y. Zhou, N. Lachman, M. Lin, D. Bhattacharya, K. K. Gleason, B. L. Wardle, Q. M. Zhang, *Electrochim. Acta* **2013**, *112*, 522.

[20] G. Yu, X. Xie, L. Pan, Z. Bao, Y. Cui, *Nano Energy* **2013**, *2*, 213.

[21] G. A. Snook, P. Kao, A. S. Best, *J. Power Sources* **2011**, *196*, 1.

[22] N. Festin, C. Plesse, P. Pirim, C. Chevrot, F. Vidal, *Sensors Actuators, B Chem.* **2014**, *193*, 82.

[23] R. R. Ferlita, D. Phipps, J. Safarik, D. H. Yeh, *Environ. Prog.* **2008**, *27*, 204.

[24] B. Anothumakkool, A. T. Torris, S. Veeliyath, V. Vijayakumar, M. V. Badiger, S. Kurungot, *ACS Appl. Mater. Interfaces* **2016**, *8*, 1233.

Author Manuscript

This article is protected by copyright. All rights reserved.

[25] W. E. Tenhaeff, K. K. Gleason, *Chem. Mater.* **2009**, *21*, 4323.

[26] A. C. Macmillan, T. M. Mcintire, S. A. Epstein, S. A. Nizkorodov, *J. Phys. Chem. C* **2014**, *118*, 29458.

[27] Q. Lv, S. Wang, H. Sun, J. Luo, J. Xiao, J. Xiao, F. Xiao, S. Wang, *Nano Lett.* **2016**, *16*, 40.

[28] B. Xie, C. Yang, Z. Zhang, P. Zou, Z. Lin, G. Shi, Q. Yang, F. Kang, C. P. Wong, *ACS Nano* **2015**, *9*, 5636.

[29] X. Xiao, X. Peng, H. Jin, T. Li, C. Zhang, B. Gao, B. Hu, K. Huo, J. Zhou, *Adv. Mater.* **2013**, *25*, 5091.

[30] G. Sun, X. Zhang, R. Lin, J. Yang, H. Zhang, P. Chen, *Angew. Chem. Int. ed.* **2015**, *54*, 4651.

[31] L. Yuan, B. Yao, B. Hu, K. Huo, W. Chen, J. Zhou, *Energy Environ. Sci.* **2013**, *6*, 470.

[32] Y. Su, Y. Fu, J. Yan, Z. Chen, B. Mao, *Angew. Chem. Int. ed.* **2009**, *121*, 5250.

[33] G. Leung, L. Smith, J. Lau, B. Dunn, C. On Chui, *Nanotechnology* **2016**, *27*, 35204.

[34] P. Kovacik, G. Del Hierro, W. Livernois, K. K. Gleason, *Mater. Horiz.* **2015**, 221.

Author Manuscript

This article is protected by copyright. All rights reserved.

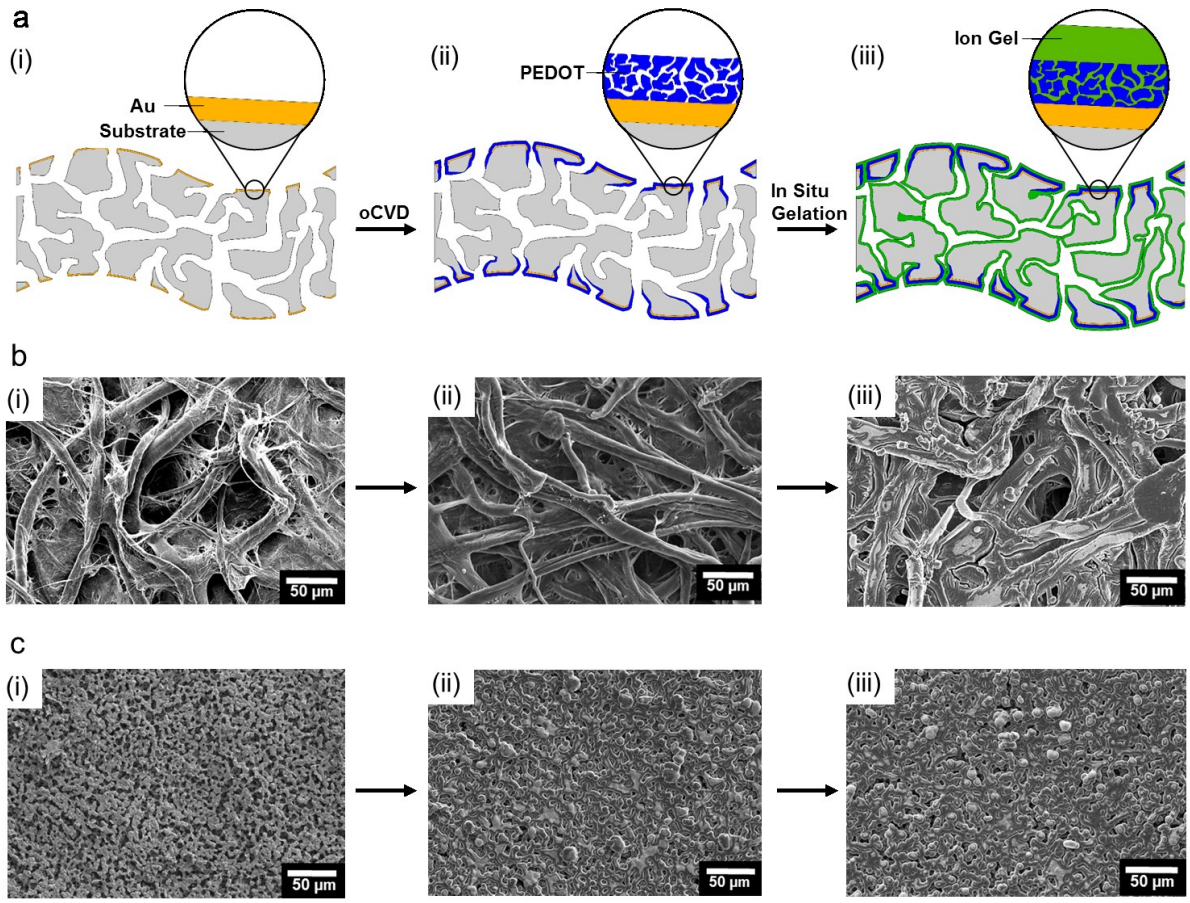


Figure 1. a) Schematic illustrations of the intermediate/final configurations of a vapor-printed solid-state SC (i-iii) after being treated by fabrication steps i-iii, respectively. The gray color indicates porous substrate; the gold color indicates gold current collector; the blue color indicates pseudo-capacitive material PEDOT; the green color indicates ion gel electrolyte. b, c) SEM images (i-iii) of the FP substrate (b) and the NM substrate (c) after steps i-iii, respectively.

Author

This article is protected by copyright. All rights reserved.

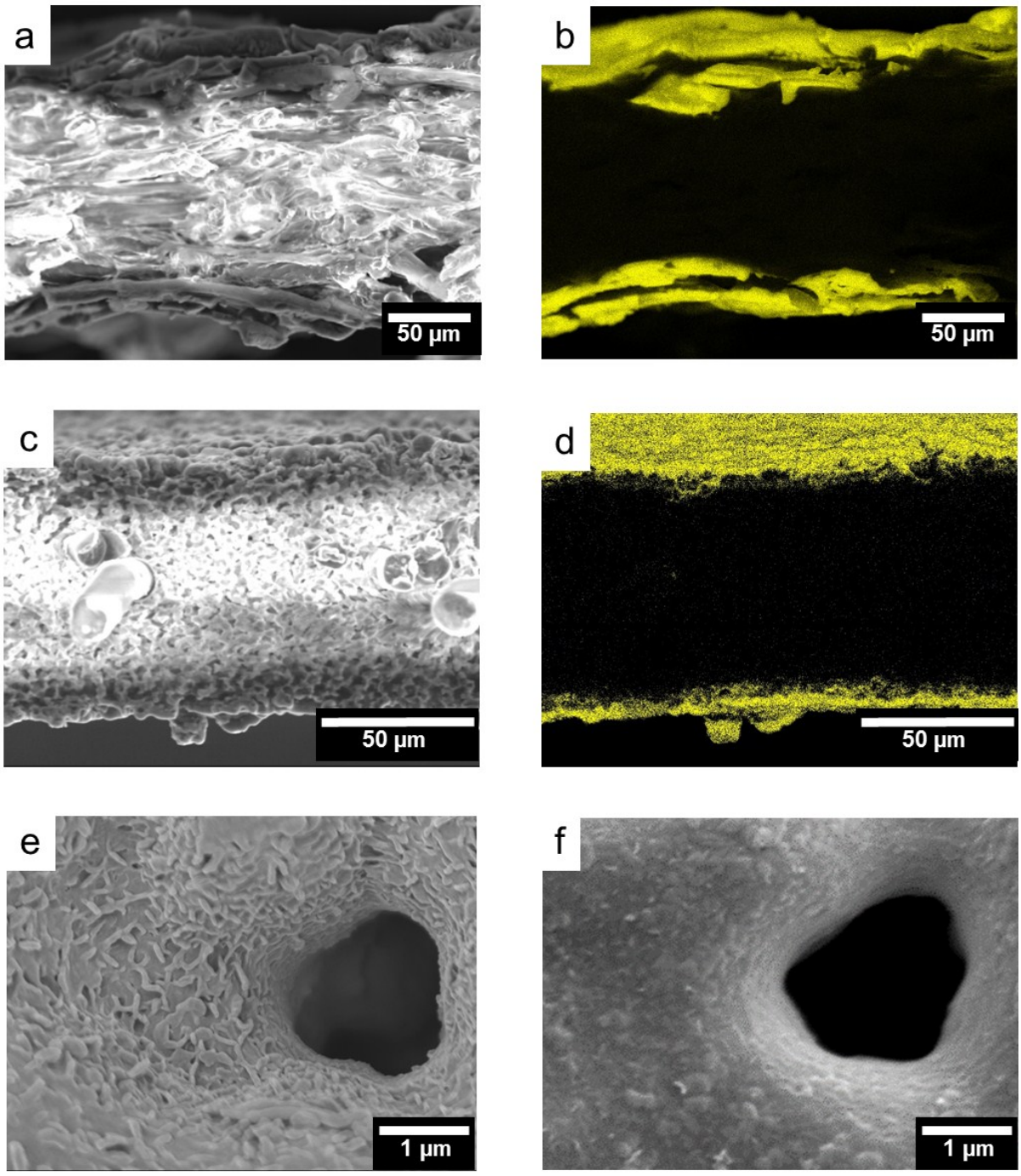


Figure 2. Cross-sectional SEM image (a) and EDS elemental map of sulfur (b) for the FP with oCVD electrodes. Cross-sectional SEM image (c) and EDS elemental map of sulfur (d) for the NM with oCVD

Aut

This article is protected by copyright. All rights reserved.

electrodes. High-resolution SEM images of PEDOT surface before (e) and after (f) in situ ion gel electrolyte synthesis.

Author Manuscript

This article is protected by copyright. All rights reserved.

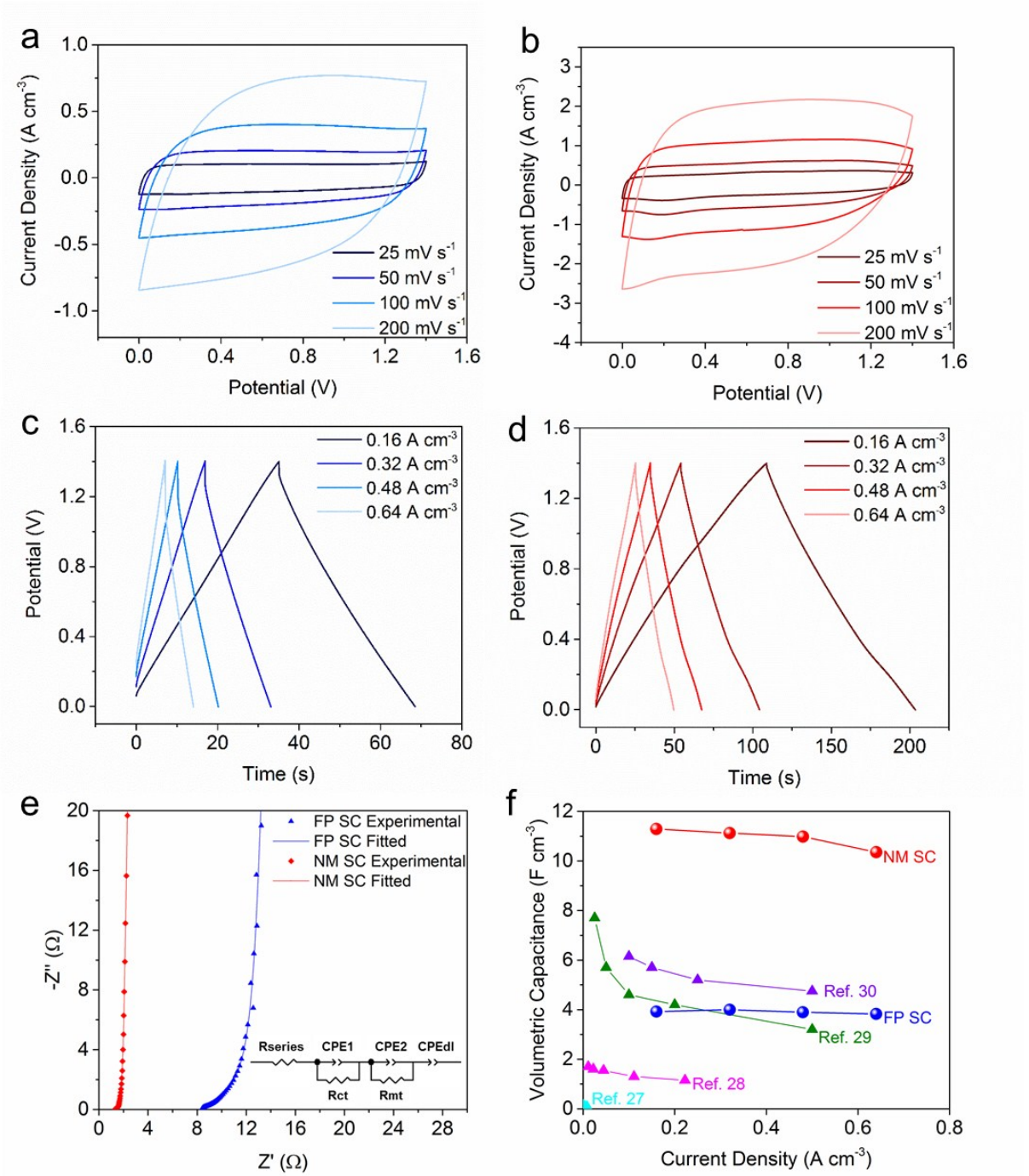


Figure 3. CVs of the FP-based SC (a) and the NM-based SC (b) at various scan rates. GV curves of the FP-based SC (c) and the NM-based SC (d) at various current densities. e) Nyquist plots of the

This article is protected by copyright. All rights reserved.

1.25×1.25 cm^2 FP- and NM-based SCs, and the fitted plots using the equivalent circuit shown in the inset. f) Volumetric capacitance of the FP and NM-based SCs compared to state-of-the-art performances.

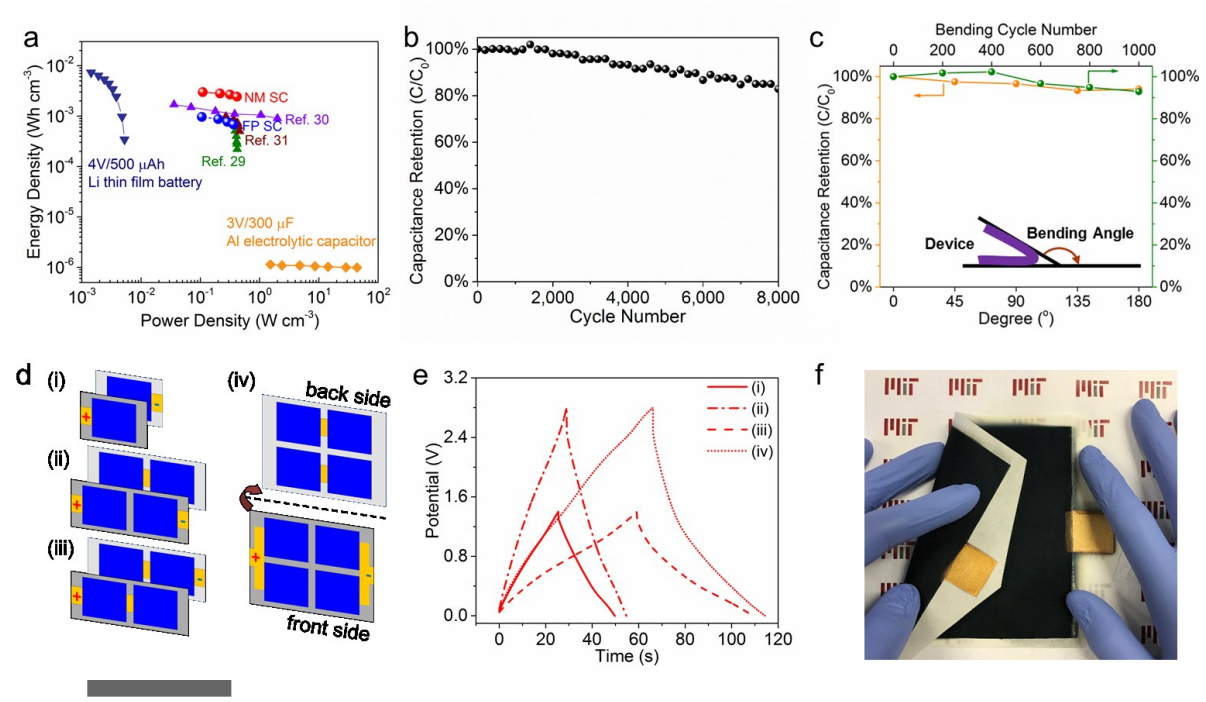


Figure 4. a) Ragone plot of FP and NM-based SCs. Data for lithium thin film battery and electrolyte capacitor are reproduced from Ref. [2]. b) Capacitance retention of a typical vapor-printed SC using GV. c) The orange color: capacitance retention of a vapor-printed SC at various bending angle (bending radius = 3 mm). The olive color: capacitance retention of a vapor-printed SC as a function of bending cycle number (bending radius = 3 mm, angle = 90°). d) Front-side and back-side pattern for monolithic devices for single cell (i), 2 cells connected in series (2S, ii), 2 cells connected in parallel (2P, iii), and series/parallel connection of four cells (2S2P, iv). The gold color represents the regions

This article is protected by copyright. All rights reserved.

with the gold current collector only; the blue color indicates oCVD PEDOT on top of the gold current collector. The devices would be imaginarily flipped along x-axis (dashed line), in order to display the patterns on both sides. e) GV curves of NM-based single cell (i), 2S (ii), 2P (iii), and 2S2P (iv) at 0.64 A cm^{-1}. f) Image of a large-area FP-based SC (12×12 cm^2).

A monolithically integrated supercapacitor is demonstrated to give high energy and power densities while avoiding delamination when being flexed. It relies on vapor deposited poly(3,4-ethylenedioxythiophene) electrodes that penetrate partially into both sides of a paper/membrane substrate, leaving the substrate's interior as separator. The electrodes conform to the substrate's outer texture, resulting in their large surface area for fast ion transport.

Keyword: chemical vapor deposition, supercapacitors, printed electronics, conducting polymers, electrode-electrolyte interfaces

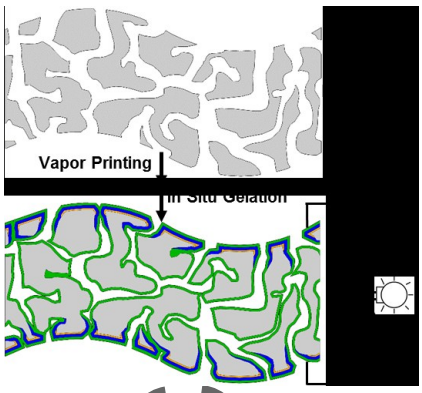
Andong Liu, Peter Kovacik, Nolan Peard, Wenda Tian, Hilal Goktas, Jonathan Lau, Bruce Dunn and Karen K. Gleason*

Monolithic Flexible Supercapacitors Integrated into Single Sheets of Paper and Membrane via Vapor Printing

ToC figure

Author Manuscript

This article is protected by copyright. All rights reserved.



Author Manuscript

This article is protected by copyright. All rights reserved.

Copyright WILEY-VCH Verlag GmbH & Co. KGaA, 69469 Weinheim, Germany, 2016.

Supporting Information

Author Manuscript

Monolithic Flexible Supercapacitors Integrated into Single Sheets of Paper and Membrane via Vapor Printing

*Andong Liu, Peter Kovacik, Nolan Peard, Wenda Tian, Hilal Goktas, Jonathan Lau, Bruce Dunn and Karen K. Gleason**

Experimental Methods

Deposition of oCVD PEDOT electrode: The oCVD process procedure and the reactor configuration are described in detail elsewhere.[1] Briefly, 3,4-ethylenedioxythiophene monomer (Sigma-Aldrich, 97%) was evaporated at 140 ^{o}C and metered at ~2 sccm. $FeCl_3$ oxidant (Sigma-Aldrich, 97%) was controllably evaporated from a resistively heated crucible at ~230 ^{o}C. The total pressure was maintained ~1 mTorr. Both sides of the substrate were covered by shadow masks in intimate contact for in situ patterning. The shadow masks were cut from paper stock (Staples) by a square punch (1.25×1.25 cm^2) and a razor blade. The substrate with shadow masks was maintained at upright position in the reactor so that both sides of the substrate were exposed to the oCVD precursors. The reaction was allowed for ~90 minutes and repeated six times. Last, samples were thoroughly rinsed by methanol (Sigma-Aldrich, 99.8%).

This article is protected by copyright. All rights reserved.

Device fabrication: Cellulose filter paper and commercially available nylon membrane (pore size ~5µm) were treated by O_2 plasma (Harrick Scientific, 29.6W) for 3 minutes to create surface hydroxyl groups. Immediately after plasma treatment, the substrates were placed into a clean beaker containing (3-mercapto-propyl)-trimethoxysilane (Sigma-Aldrich, 95%)/isopropanol (Sigma-Aldrich, 99.5%) (=1/50, v/v) solution. The silanization was allowed overnight to graft thiol groups for enhanced adhesion between the substrate and the gold layer. The substrates were then washed by anhydrous isopropanol and dried under vacuum for 5 hours. The silanized substrates were shadow masked and coated with gold by sputtering (Polaron SC7640, plasma current ~20 mA) for 960s each side. PEDOT electrodes were deposited via oCVD on both sides of the masked substrates as described above. N, N-dimethylacrylamide (DMAA, Sigma-Aldrich, 99%), ethylene glycol dimethylacrylate (EGDMA, 2 vol% based on DMAA, Sigma-Aldrich, 98%), 4,4'-azobis(4-cyanovaleric acid) (ABCVA, 1 wt% based on the monomers, Sigma-Aldrich, 98%) were mixed with ionic liquid 1-ethyl-3-methylimidazolium tetrafluoroborate ([EMIM] [BF_4], 300 vol% based on the monomers, Sigma-Aldrich, 99.0%) under vigorous stirring until the ABCVA powder appeared fully dissolved. The precursor solution was drop-cast on the substrate with PEDOT electrodes, and infiltrated the electrodes spontaneously. Excessive solution was absorbed by wipers. The wetted samples were heated by a heat gun (Master Appliance Varitemp) until the samples appeared dry, and immediately placed in an oven at 90°C overnight to form solid-state devices. For comparison, a NM-based SC was made with H_2SO_4-PVA electrolyte prepared according to a previously reported method.[2] Briefly, 2 g H_2SO_4 was mixed with 20 mL deionized water and heated up to 85 °C under vigorously stirring. Subsequently 2 g PVA (polyvinyl alcohol, molecular weight 89,000-98,000, Sigma-Aldrich) powder was added to the solution. The solution was stirred until it appeared clear. The NM with printed

Author Manuscript

This article is protected by copyright. All rights reserved.

PEDOT electrodes was immediately dip-coated in the hot solution. The electrode coated by the solution was left in a fume hood overnight to allow to dry.

Electrode, electrolyte and substrate characterization: The cross-sections of the substrates with PEDOT coatings were obtained using Cryo-Snap method described in detail elsewhere.[3] Briefly, a sample was cut into a thin strip and subsequently submerged in water in a glass tube. The tube containing water and sample was slowly submerged into liquid nitrogen, and removed after being frozen for 2 minutes. The glass tube was immediately scored at the location of interest and snapped into two. The fractured samples were dried under vacuum overnight. For cross-section imaging and EDS, the fractured surfaces were coated by carbon (Denton Desk II, ~ 35A) to increase conductivity. The SEM images and EDS elemental map were obtained using JOEL JSM-6010LA. High-resolution FE-SEM images were obtained using JOEL JSM-6700F. The XPS spectra were acquired on a SSX-100X-probe (Surface Science Instruments) spectrometer with a monochromatized Al Kα source operated at 1486.6 eV. The pass energy was 150 V for survey scans. The pressure during analysis was kept under 1.6×10^{-9} Torr. The sample charge was neutralized by a 1 eV electron beam flood gun. CasaXPS software was used to analyze the spectra. ATR-FTIR measurement was performed on a Nicolet iS50 FT-IR Spectrometer (Thermo Scientific) equipped with a MCT/A detector cooled by liquid nitrogen. Nitrogen adsorption/desorption was conducted on an automatic volumetric adsorption analyzer (Micromeritics ASAP2020).

Author Manuscript

This article is protected by copyright. All rights reserved.

Device characterization: CV and GV measurements of the samples were conducted in a two electrode system using an electrochemistry workstation (CHI660D, CH Instrument). Toothless alligator clips (Mueller, nickel-plated steel) were used to connect the workstation to the protruding part of the gold current collector (indicated by +/- in Figure 4d). A small piece of carbon paper was inserted in between the alligator jaw and the gold protrude to enhance the electrical contact. EIS measurements were performed on a potentiostat (VMP3, Bio-Logic). EC-Lab and ZView software were used for the circuit fitting. A small piece of platinum foil was inserted in between the alligator jaw and the gold protrude to enhance the electrical contact. Compressive flexing test for the devices was performed using an ADMET micro EP miniature testing machine. The GV curves were used to calculate the specific volumetric capacitances, energy density and power density as follows:

Specific volumetric capacitance of the SC C_V (F cm^{-3}) was calculated using the equation

$$C_{\mathrm{V}} = \frac{I_{\mathrm{D}} \cdot \Delta t}{V_{\mathrm{SC}} \cdot \Delta V}$$

where I_D (A) is the discharge current, Δt (s) is the discharging time, V_{SC} (cm^3) is the volume of the entire SC device, and ΔV (V) is the cell voltage.

Specific gravimetric capacitance of the electrode $C_{electrode}$ (F g^{-1}) was calculated according to the formula

$$C_{\mathrm{electrode}} = \frac{4 I_{\mathrm{D}} \cdot \Delta t}{m \cdot \Delta V}$$

where m (g) is the total mass of both electrodes determined by measuring the mass change of the substrate before and after PEDOT deposition.

Author Manuscript

This article is protected by copyright. All rights reserved.

The volumetric energy density of the SC E_V (Wh cm^{-3}) was obtained from the equation

$$E_V = \frac{C_V \cdot \Delta U^2}{2 \times 3600}$$

where ΔU (V) is the operating potential window, equal to ΔV subtracting the *IR* drop (V).

The power density P_V (W cm^{-3}) was calculated from the formula

$$P_V = \frac{3600 E_V}{\Delta t}$$

Supporting Figures

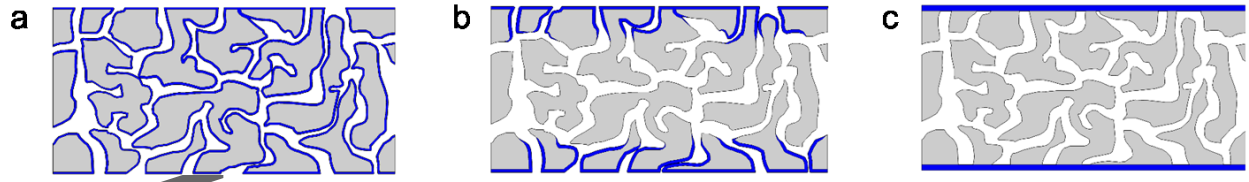


Figure S1. Schematics of porous substrates coated by PEDOT with full conformality (a), partial conformality (b), and non-comformality (c).

Author Manuscript

This article is protected by copyright. All rights reserved.

Author Manuscript

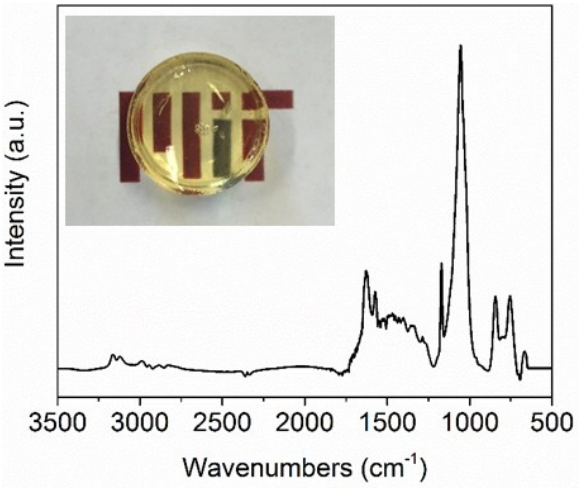
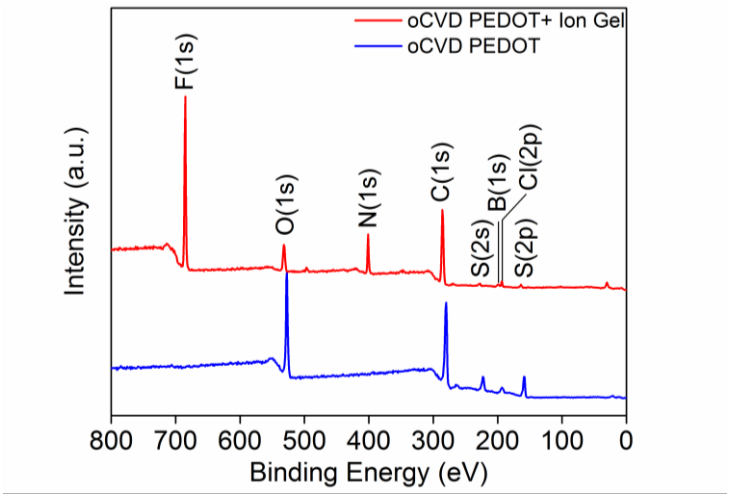


Figure S2. FTIR spectrum of ion gel electrolyte. Inset: image of a freestanding ion gel pellet. The sharp band at 1630 cm^{-1} is caused by the carbonyl stretch of pDMAA.[3] For [EMIM] [BF_4], stretching bands of the imidazolium ring are found at 1574 cm^{-1} and 1171 cm^{-1}.[4] The broad peak centered at 1055 cm^{-1} and the sharp peaks around 1286 cm^{-1} and 756 cm^{-1} are attributed to the stretching modes of the tetrafluoroborate anion.



This article is protected by copyright. All rights reserved.

Figure S3. XPS spectra of oCVD PEDOT surface before (blue) and after (red) in situ ion gel electrolyte generation.

Manuscript

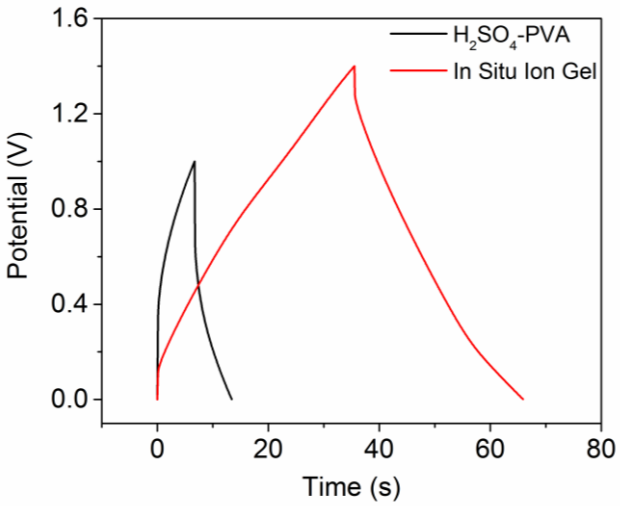
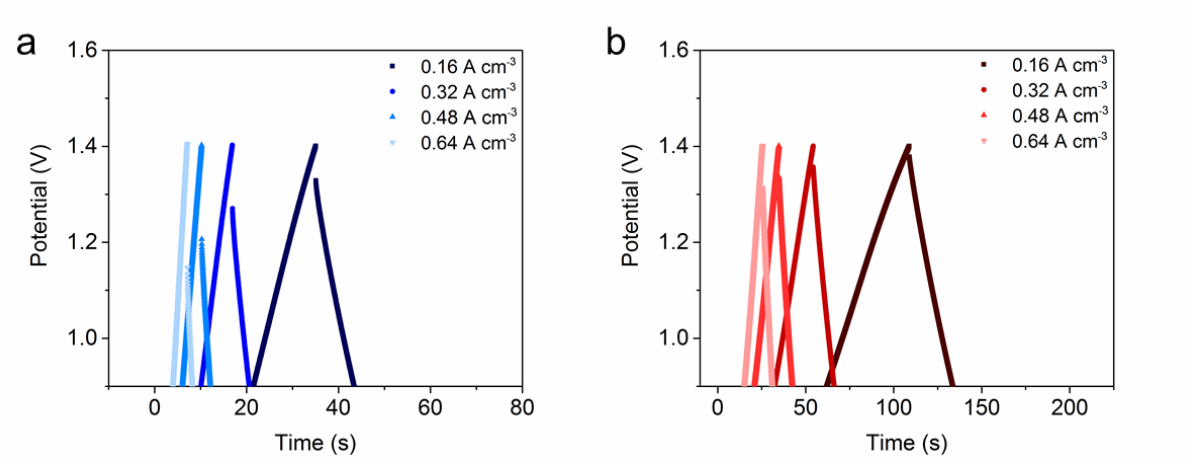


Figure S4. GV curves of a NM-based SC with conventional H_2SO_4-PVA gel electrolyte and in situ synthesized ion gel electrolyte at 0.48 A cm^{-3}.



This article is protected by copyright. All rights reserved.

Figure S5. Enlarged view of IR drops for the FP-based (a) and NM-based (b) SCs at various current densities.

Author Manuscript

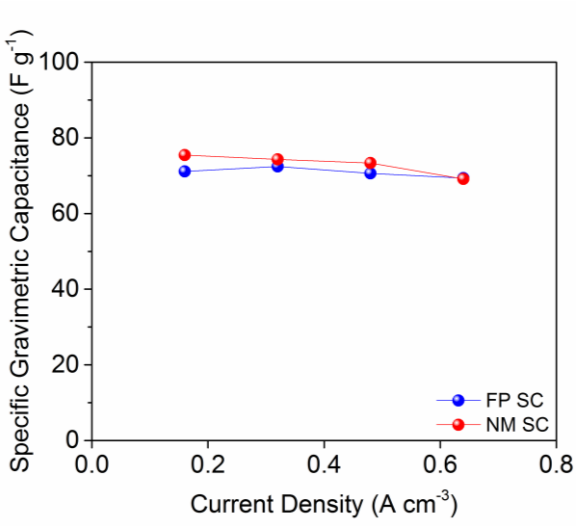


Figure S6. Specific gravimetric capacitance of PEDOT in the FP-based and NM-based SCs at various current densities. By measuring the mass change of the substrates before and after PEDOT deposition, the total mass of PEDOT electrodes are determined to be 2.9 mg for the FP-based SC and 3.1 mg for the NM-based SC.

This article is protected by copyright. All rights reserved.

References

[1] S. G. Im, K. K. Gleason, *Macromolecules* **2007**, *40*, 6552.

[2] C. Meng, C. Liu, L. Chen, C. Hu, S. Fan, *Nano Lett.* **2010**, *10*, 4025.

[3] R. R. Ferlita, D. Phipps, J. Safarik, D. H. Yeh, *Environ. Prog.* **2008**, *27*, 204.

[4] W. E. Tenhaeff, K. K. Gleason, *Chem. Mater.* **2009**, *21*, 4323.

[5] A. C. Macmillan, T. M. Mcintire, S. A. Epstein, S. A. Nizkorodov, *J. Phys. Chem. C* **2014**, *118*, 29458.

Author Manuscript

This article is protected by copyright. All rights reserved.